Bioelectrochemistry 168 (2026) 109137

Contents lists available at ScienceDirect

Bioelectrochemistry

journal homepage: www.journals.elsevier.com/bioelectrochemistry

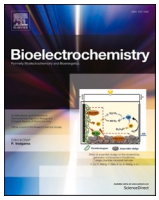

High sensitivity perovskite-tagged nanobody electrochemiluminescent immunosensor for spike (S1) protein biomarker-based persistent viral reservoir detection

Jaymi January [a,b,*], Olivier Zwaenepoel [b], Nelia Sanga [a], Jan Gettemans [b,**], Emmanuel Iwuoha [a,**]

[a] SensorLab (University of the Western Cape Sensor Laboratories), University of the Western Cape, 4th Floor Chemical Sciences Building, Robert Sobukwe Road, Bellville, 7535 Cape Town, South Africa
[b] Department of Biomolecular Medicine, Nanobody Lab, Faculty of Medicine and Health Sciences, Ghent University, Tech Lane Ghent Science Park 75, 9052 Ghent, Belgium

ARTICLE INFO

Keywords:
Disease biomarker detection
electrochemiluminescence (ECL)
nanobody-based biosensor
spike protein (S1)
sandwich immunosensor
persistent viral reservoirs

ABSTRACT

Persistent viral reservoirs (PVR) of SARS-CoV-2 (or long COVID-19) and latent COVID-19 disease have been of great concern to clinicians. Several studies have identified spike protein (S1) as a definitive biomarker for the early detection of persistent viral reservoirs and latent COVID-19. A novel sandwich-format electrochemical immunosensor integrating a nanocomposite material was engineered for rapid and sensitive latent COVID-19 detection. The platform structure, AuSPE||strep|Nb_1|BSA|biotin|S1|strep-$LiSmZrO_3$-Nb_2 + BSA (AuSPE = gold screen-printed electrode, strep = streptavidin-thiol, Nb_1 = primary nanobody, Nb_2 = secondary nanobody, BSA = bovine serum albumin, and spike (S1) protein = S1), featured a disposable AuSPE modified with strep to anchor a biotinylated camelid Nb_1 specific to the spike protein. A Nb_2 conjugated to streptavidin-labelled $LiSmZrO_3$ perovskite completed the sandwich complex, enhancing both affinity and signal transduction. Electrochemical responses of the sensor were studied via electrochemiluminescent (ECL) signal transduction. The S1-sensitive sandwich immunosensor had a detection range of 0–1000 pg mL^{-1} with a limit of detection of 0.04 pg mL^{-1} via ECL. As feasibility studies, commercial spike protein in buffered solutions and human serum, highlighting the potential for the immunosensor to be used in SARS-CoV-2 patients and PVRs. The nanobody sandwich immunosensor showed excellent stability, selectivity, sensitivity, and reproducibility. The immunosensor serves as a broad PVR for a SARS-CoV-2 screening tool, detecting elevated S1 levels to enable early, targeted diagnostics.

1. Introduction

Persistent viral reservoirs (PVRs) of Severe Acute Respiratory Syndrome Coronavirus 2 (SARS-CoV-2) refer to specific tissues or cells, such as the brain, gastrointestinal tract, lungs, lymphoid tissue, fat, and immune cells like monocytes, where viral RNA, proteins, or antigens can remain long after the acute infection has resolved [1]. Although SARS-CoV-2 does not establish classical viral latency, it may persist at low, subclinical levels in these reservoirs, contributing to a state often described as latent or chronic coronavirus disease (COVID). This persistent presence is believed to be a key driver of long COVID symptoms, due to continuous immune stimulation or residual antigenic exposure [2]. Standard diagnostic tests often fail to detect the virus in these hidden sites, making detection and characterization of PVRs critical. Identifying these reservoirs can help improve diagnostic accuracy for long COVID, guide the development of targeted antiviral or immunomodulatory therapies, and inform vaccine strategies [3]. Moreover, detecting persistent viral components in blood or tissue could serve as valuable biomarkers for monitoring disease progression and therapeutic response. Currently, new technological advancements are underway to

* Corresponding author at: SensorLab (University of the Western Cape Sensor Laboratories), University of the Western Cape, 4th Floor Chemical Sciences Building, Robert Sobukwe Road, Bellville, 7535 Cape Town, South Africa.
** Corresponding authors.
E-mail addresses: 3651284@myuwc.ac.za (J. January), Jan.Gettemans@ugent.be (J. Gettemans), eiwuoha@uwc.ac.za (E. Iwuoha).

https://doi.org/10.1016/j.bioelechem.2025.109137
Received 1 August 2025; Received in revised form 9 October 2025; Accepted 10 October 2025
Available online 12 October 2025

address the limitations of existing PVR of SARS-CoV-2 (or long COVID-19) and latent COVID-19 detection methods. Most of the ELISA systems that are currently being employed rely on antibodies, which are the main components of the immune system's recognition system [4]. Although antibodies are commonly used as a routine part of the development process, they have several drawbacks, such as their large, complex structure and size, which can cause various defects. Additionally, one of the main drawbacks of using polyclonal antibodies is their variability in batch-to-batch conditions. This can prevent the development of protein engineering [5]. Another issue with antibodies is random attachment to the support, which can lead to partial loss of function, such as binding via the antigen site or denaturation upon adsorption. Due to the technological advancements that have occurred in the field of biologics, there is a growing movement toward the use of recombinant antibodies and non-antibody binding proteins. This method allows the continuous production of a stable protein with no variation. Moreover, the obstacles that occur when using conventional antibodies can be overcome by a single entity that has the full antigen-binding properties of a functional antibody; this is known as a nanobody (Nb). These new products are designed to carry a variable domain of heavy-chain antibodies found in animals from the *Camelidae family* [6]. When compared to conventional antibodies, these nanobodies have several advantages, such as higher thermostability and flexibility, improved solubility, ease of recombinant expression, and the ability to interact with a variety of antigens [7]. Nbs have a shorter half-life in vivo, which allows the kidneys to quickly clear the unbound portion of the product. They can also be produced in large quantities using various types of bacteria and yeast [6]. It is also more affordable to develop and maintain these types of antibodies than to produce multiple types of conventional antibodies. Therefore, Nbs might solve several problems, since they can detect clinically relevant antigens with good sensitivity even under harsh conditions, creating many opportunities to diagnose diseases or infections and treat them. As such, they have been regarded as outstanding features in the field of therapeutic [8] and diagnostic [9] applications.

In recent years, there has been growing interest in biosensors for detecting disease markers associated with persistent viral reservoirs [10–16]. These methods have various advantages, such as a wide linear range, high sensitivity, and reproducibility, which endow these methods with broad prospects of extensive application in the diagnosis and treatment of disease. Extensive research has been undertaken to improve the efficiency, accuracy, and sensitivity of biosensors. One of the prominent factors is the incorporation of nanomaterials into the system. However, to date, there are very few that incorporate perovskite nanomaterials. Perovskite nanomaterials have become an emerging material due to their unique properties. Although perovskite nanomaterials have been applied in various biosensing platforms for cancer and kidney biomarkers [8–10], their application in SARS-CoV-2 antigen-antibody sensors remains largely unexplored. Wang et al [17], reported on the use of encoded probes that were based on DNA-$LaMnO_3$ (DNA-LMO) perovskite material. This formed their aptasensing platform for the detection of alpha-fetoprotein (AFP), carcinoembryonic antigen (CEA), and prostate-specific antigen (PSA) biomarkers. They showed that the enhanced amplification effect of their material toward the aptasensor was due to their numerous LMO-M-enriching properties. Then, Chakraborty and co-workers [14] developed an immunosensor based on nickel oxide nanoparticles modified cerium-copper oxide perovskite for the detection of acute kidney injury, specifically lipocalin 2. They obtained a detection limit of 4.23 pg mL^{-1} and highlighted that the combination of chemically modified perovskite oxide and transition metal oxide nanoparticles results in a significantly improved electrochemical conductivity of the sensing electrode. Likewise, Yu et al [18], reported on a photoelectrochemical (PEC) immunoassay that was enhanced using a perovskite-based (lanthanide-doped bismuth ferrite/reduced graphene oxide/tungsten oxide nanohybrids) photo-sensing material. They showed that the use of the perovskite material enabled the transferred charges to move in the circuit, which allowed for a separation of the photo-generated holes and electrons. They were able to sensitively detect PSA with a detection limit of 49.4 pg mL^{-1}. These research articles highlight the fact that the use of perovskite materials in sensing applications is possible, further confirming the benefits that these materials offer, such as excellent electrochemical stability, ferroelectricity, superconductivity, and excellent catalytic activity. These results may be crucial to the area of improving detection techniques to diagnose and prevent diseases. In this study, the perovskite nanomaterial used was $LiSmZrO_3$. Previous studies have demonstrated the superior electrochemical properties of this material. January et al [19] recently showed its effectiveness in amplifying electrochemical signals for interferon-gamma detection, confirming its stability and sensitivity in biosensing. Likewise, rare-earth-doped Li_2ZrO_3 perovskites have been reported to enhance electrocatalytic efficiency and durability [20]. The successful application of rare-earth-modified materials in sensitive electrochemical biosensors [21] further supports the rationale for employing $LiSmZrO_3$. Taken together, these findings highlight that $LiSmZrO_3$ is not only structurally stable but also provides distinct electrochemical advantages, making it an excellent choice for electrochemiluminescent (ECL) signal amplification in biosensor development.

Similarly, nanobody-based sensors have shown promise for SARS-CoV-2 detection [16–20], but existing designs typically rely on antibodies or hybrid formats, and few adopt a sandwich-type configuration. To date, no report has combined nanobodies with perovskite nanomaterials in an electrochemiluminescent sandwich immunosensor for detecting the S1 protein as a biomarker of persistent viral reservoirs. Maher et al [22] reported on the use of lateral flow test (LFT) strips based on dual gold conjugates (Au-Nbs as the detector probe, and Au-ACE 2 as the capture probe) for the detection of SARS-CoV-2S protein. Their results show that the conjugation resulted in an exaggerated signal intensity and an improved sensitivity, specificity, and limit of detection when compared to monoclonal antibody (mAb)-based strips. Yame He and co-workers [23] then reported on the use of nanobodies in SARS-CoV-2 whole-cell biosensors. They made use of nanobody-displayed yeast as the capture probe and AuNPs functionalized HRP conjugated to anti-SARS-CoV-2 mAb as their signalling probe. They were able to detect SARS-CoV-2S protein with a limit of 0.037 μg mL^{-1} and showed that through the expression of nanobodies, the engineered yeast can quickly purify and concentrate SARS-CoV-2-related S proteins found in complex matrices. Similarly, Kamel et al [24] developed a protocol based on a sandwich enzyme-linked immunosorbent assay. In their protocol, they made use of recombinant S1 mAb and Au-conjugated Nb's as their antigen capture and detection probes, respectively. After the AuNPs functionalization, the reaction of these conjugates with free nanobodies was compared. The results of their study revealed that the use of AuNPs Nbs significantly increased the absorbance reading, ultimately resulting in an impressively elevated sensitivity in both saliva and nasal swabs. Then, Yun Chen and co-workers [25] fabricated a nanobody-based photoelectrochemical immunoassay for SARS-CoV-2S protein and used Au@TiO_2 photoactive nanomaterial as their sensing platform. The interaction of the TiO spheres and the AuNPs directly immobilized the Nb, leading to a low detection limit of 5 fg mL^{-1}. They highlighted that the small size of the Nb, coupled with a higher density on the PEC immunosensor, improved the signal-to-noise ratio of the instrument. This helped reduce the detection limit and obtain a sensitive analysis. Lastly, Pagneux et al [26] reported on an Nb-functionalized voltametric system for the detection of whole SARS-CoV-2 viral particles (RBD). An Au-modified surface was used as their sensing platform. They found that the incorporation of their anti-fouling technique and the nanobody's surface orientation were the underlying factors in this project's success. In addition, the device's sensitivity exceeded the reverse transcription polymerase chain reaction's detection rate. They reported that the only possible drawback is the device's ability to detect the virion in the presence of mutant RBDs, which can affect the epitopes of the Nb. However, the sensitization of the device and its chosen ligand prevented

this issue. Based on the information obtained, it is evident that the research area of nanobodies' functionality in biosensors is limited, and current approaches either exploit nanobodies for SARS-CoV-2 detection without advanced signal amplification or nanomaterials, such as perovskites. This leaves a clear gap in developing highly sensitive platforms that integrate both strategies to enable ultra-low-level detection of the S1 protein as a biomarker of persistent viral reservoirs, a critical unmet need in long COVID diagnostics. This work addresses this gap through three unique innovations: (i) the first integration of perovskite nanomaterials ($LiSmZrO_3$) into a nanobody-based immunosensor for SARS-CoV-2 detection, (ii) direct application to detecting the S1 protein as a biomarker of persistent viral reservoirs, an area currently lacking reliable diagnostic tools, and (iii) the use of nanobodies as both capture and detection probes in a sandwich configuration using electrochemiluminescence, ensuring high selectivity and reduced steric hindrance. By addressing the limitations of conventional antibody-based methods, the sensor enables sensitive and reliable detection of persistent viral antigens, offering a novel diagnostic tool for monitoring post-acute SARS-CoV-2 infection.

The goal of this study is to develop and evaluate a highly sensitive electrochemiluminescent immunosensor that employs perovskite nanomaterials as signal enhancers and nanobodies as selective recognition elements for the detection of the spike protein. Gold screen-printed electrodes (AuSPE) modified with streptavidin-thiol (strep) were employed to immobilize the biotinylated primary nanobody (Nb_1), functioning as the capture probe. Biotin-streptavidin interaction ensures proper orientation of each nanobody. Then, the secondary nanobody was labelled with a perovskite-type nanomaterial to serve as a signal amplifier and detection probe. This was done by tagging the perovskite nanomaterial ($LiSmZrO_3$) with streptavidin-thiol to allow for a non-covalent binding to the secondary biotinylated nanobody (Nb_2). The high affinity between streptavidin and biotin enables high coupling efficiencies. Additionally, the use of a strep-labelled $LiSmZrO_3$ tag reduced steric hindrance and strengthened the interaction between the S1 and the detection nanobody, leading to improved sensitivity. To test the immunosensor's performance, different concentrations of S1 were introduced. The fabricated immunosensor exhibited a wide linear range, a low detection limit, and showed comparable analytical performance. By targeting the S1 protein as a biomarker of persistent viral reservoirs, this sensor aims to enable accurate, low-level detection of residual viral antigens associated with long COVID, thereby contributing to improved diagnostics and monitoring of post-acute SARS-CoV-2 infection.

2. Materials

2.1. Chemicals and sample preparation

The following analytical-grade reagents, used without further purification, included 70 % isopropanol, EDC [1-ethyl-3-(3-dimethylaminopropyl) carbodiimide hydrochloride], NHS [N-hydroxysuccinimide], Dulbecco's phosphate-buffered saline (10 mM DPBS, pH 7.4), bovine serum albumin (BSA), human serum (obtained from male AB plasma and stored at −80 °C) and 1 mg mL^{-1} streptavidin-thiol were all purchased from Sigma Aldrich (South Africa). The $LiSmZrO_3$ perovskite nanomaterial used in this study was not re-synthesized but employed as received from our previously synthesized and fully characterized batch. Its structural, morphological, and compositional properties have been comprehensively reported in our earlier work [19,20], confirming the successful formation of phase-pure $LiSmZrO_3$ with characteristic perovskite features. SARS-CoV-2 spike RBD-His recombinant protein was purchased from Sino Biological Europe GmbH (Europe). The production of both nanobodies Nb1RBDnoCys (Nb_1) and Nb2RBDNoCys (Nb_2) is done via cloning the cDNA into an *Nco*I-digested pET22b vector. Thereafter, a double transformation is performed using the pET22b plasmid and the BirA plasmid for in vivo biotinylation of the nanobodies. Purification of both nanobodies was carried out using nickel (Ni) affinity resin, targeting their His_6-tags. Dulbecco's phosphate-buffered saline (10 mM DPBS) was used as the base solution to prepare the following concentrations: 10 μg mL^{-1} of biotinylated S1 Nb1 (Nb_1), 10 μg mL^{-1} of biotinylated Nb2 (Nb_2), 100 μg mL^{-1} streptavidin, and an S1 antigen stock at 5×10^3 pg mL^{-1}. Antigen working solutions ranging from 0 to 1000 pg mL^{-1} were prepared by serial dilution in DPBS. All solutions, nanobodies, streptavidin, and antigen were stored at −20 °C when not in use.

2.2. Nanobody selection

The spike protein has multiple antigenic sites, which can be categorized into seven distinct binding regions, including the receptor-binding motif (RBM), the outer surface of the RBD, and its inner surface. Research conducted by Xiaojing Chi and colleagues [27] identified three nanobodies, Nb1, Nb2, and Nb15, that exhibited cross-protective effects against the spike protein at a concentration of 0.33 μM, each displaying a unique and either overlapping or complementary neutralization profile. Among these, Nb1 and Nb2 were found to possess especially strong binding affinity and potent neutralizing capabilities. Epitope mapping revealed that although the binding sites of Nb1 and Nb2 partially overlap, they target distinct regions: Nb1 primarily engages the outer surface of the RBD, while Nb2 is directed toward the RBM. Notably, antibodies targeting the RBM tend to show the highest neutralization potency, whereas those binding the outer face of the RBD offer broader neutralization coverage. Furthermore, experiments showed that when Nb1 or Nb2 was introduced to an ACE2-saturated probe, no additional binding occurred, indicating direct competition between these nanobodies and ACE2 for the RBD. The fact that Nb1 and Nb2 recognize different, non-overlapping epitopes supports their selection for biosensor development, as their non-competitive interactions enhance assay performance and sensitivity.

2.3. Electrochemiluminescence measurements

Gold screen-printed electrodes (AuSPEs, Ref. C220AT) were purchased from Metrohm-Dropsens (Asturias, Spain) and used in the fabrication of the immunosensor. The stepwise assembly of the modified bioelectrode and its electrochemical behavior were characterized using ECL and various other electrochemical techniques. For electrochemical measurements, the modified electrodes were inserted into a screen-printed electrode connector linked to a PalmSens Trace 4.4 potentiostat (Randhoeve, GA, Houten, The Netherlands), which featured an integrated Windows 10 computer for data acquisition and analysis. ECL measurements were conducted using a CH Instruments Model 760B electrochemical workstation. The ECL signal was detected with an Oriel 70,680 photomultiplier tube (PMT), powered by an Oriel Model 70,705 high-voltage supply and connected to an Oriel Model 70,701 amplifier/recorder. The electrode modification and sensor development were initially assessed through cyclic voltammetry (CV), using a potential range from −1.5 V to 1.5 V and a scan rate of 50 mV/s. These experiments were performed at room temperature using 0.1 M PBS or 10 mM DPBS, pH 7.4 aqueous electrolytes. Thereafter, the modification steps and the immunosensor's analytical capabilities were assessed via ECL, using a potential range of 0.4 V to 1.3 V and a scan rate of 50 mV/s. All ECL experiments were performed in a light-tight enclosure using a custom-designed holder, where the three-electrode cell was positioned with the working electrode facing directly opposite a fiber optic bundle. The opposite end of the bundle was aligned with the PMT to ensure optimal light collection. Measurements were carried out in 2 mL of DPBS (0.1 M, pH 7.5) containing 50 μM $[Ru(bpy)_3]^{2+}$ and 100 mM TPA, at room temperature. ECL spectra were recorded during a cyclic voltametric scan, with the potential swept from 0.3 V to 1.3 V (vs. Ag/AgCl) at a rate of 30 mV/s. The PMT was operated at a bias voltage of −850 V throughout the measurements. All the results were analyzed using OriginPro (Version 2021, OriginLab Corporation, Northampton, MA, USA),

and baseline correction was applied with the software's built-in correction tool. To enhance signal clarity, baseline correction was performed within the software, applying either a linear or segmented model based on the characteristics of the background signal. This approach successfully eliminated non-faradaic contributions, enabling precise identification of faradaic currents related to analyte binding events.

2.4. Labelling and conjugation of $LiSmZrO_3$ with secondary nanobody (Nb_2)

Two distinct approaches were employed to functionalize the perovskite material ($LiSmZrO_3$) for conjugation with the secondary nanobody (Nb_2), involving either cysteine or streptavidin functionalization.

Approach 1: Cysteine-capped $LiSmZrO_3$ and covalent coupling with Nb_2.

To prepare cysteine-capped $LiSmZrO_3$, 5 mg of cysteine was dissolved in 50 mL of deionized water (0.1 g/L) and added dropwise to a 1 mM suspension of $LiSmZrO_3$ (15 mg), under constant stirring. The mixture was stirred for 2 h at room temperature, allowing the thiol groups of cysteine to interact with samarium ions on the nanoparticle surface. After incubation, the mixture was centrifuged to remove excess reagents, and the pellet was stored in a dark glass container at 4 °C.

For conjugation, a 1 mL solution of Nb_2 (10 μg mL^{-1}) was activated with an EDC: NHS mixture (4:1 ratio) for 15 min at 4 °C. Then, 100 μL of cysteine-capped $LiSmZrO_3$ (10 mg mL^{-1}) was added dropwise to the activated nanobody solution under vigorous stirring, followed by gentle stirring for 12 h at room temperature to facilitate covalent attachment between the thiol-functionalized nanoparticles and activated carboxyl groups on Nb_2.

Approach 2: Streptavidin-labelled $LiSmZrO_3$ and biotin–streptavidin

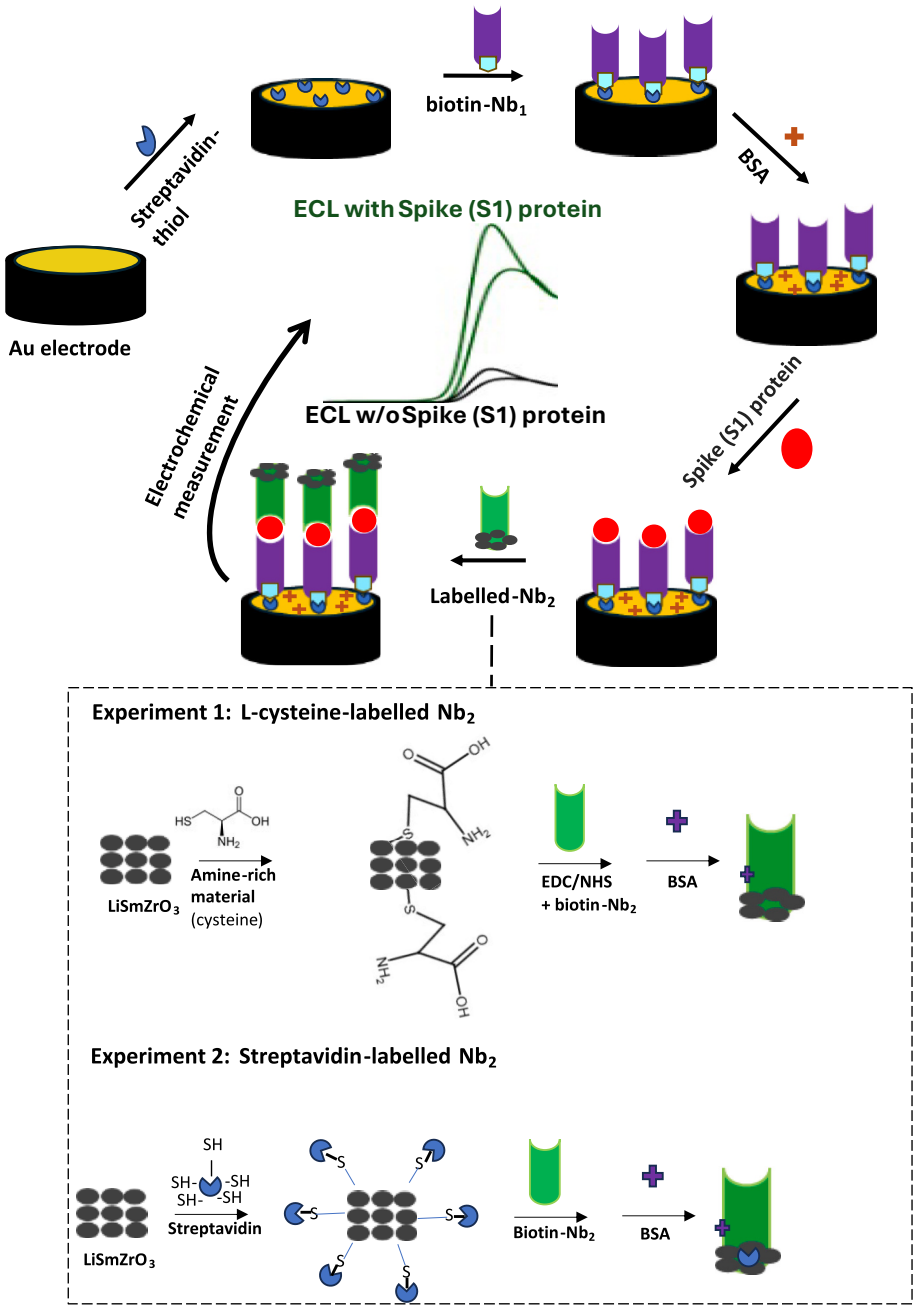

Scheme 1. Development of a perovskite-enhanced sandwich-format nanobody immunosensor employing various strategies for the detection of the spike (S1) protein target analyte.

interaction with Nb_2.

In this approach, 1 mL of 1.0 mg mL^{-1} streptavidin-thiol was added to 1 mL of $LiSmZrO_3$ (15 mg in 10 mM DPBS, pH 7.4), and the mixture was gently stirred for 30 min at room temperature to enable Au–SH binding. Excess streptavidin was removed by repeated centrifugation and washing, and the labelled nanoparticles were stored in DPBS at 4 °C.

To conjugate Nb_2, the nanobody was first biotinylated. Then, 100 μL of streptavidin-labelled $LiSmZrO_3$ (10 mg mL^{-1}) was added dropwise to 1 mL of the biotinylated Nb_2 solution (10 μg mL^{-1}) under vigorous stirring. The mixture was gently stirred for 12 h at room temperature, allowing the non-covalent binding of biotinylated Nb_2 to the streptavidin-functionalized nanoparticles.

Post-conjugation processing (Common to both approaches).

Following nanobody attachment in both approaches, 1 mL of 1 % (*w/v*) bovine serum albumin (BSA) was added to block nonspecific binding sites. After a 1 h incubation, the mixture was centrifuged at 4000 rpm to remove unbound molecules. The supernatant was discarded, and the pellet was washed with DPBS and redispersed in 0.1 M DPBS (pH 7.4). The resulting Nb_2–$LiSmZrO_3$ bioconjugates were stored at 4 °C until further use.

2.5. Sandwich-immunosensing procedure

Scheme 1 illustrates the step-by-step fabrication of the developed sandwich-type immunosensor. The process begins with the cleaning of the bare AuSPE, which is rinsed sequentially with ethanol and deionized water, followed by drying under a gentle stream of nitrogen gas. Next, 10 μL of strep solution (100 μg mL^{-1}) is drop-cast onto the electrode surface and incubated overnight at 4 °C to enable surface functionalization. After incubation, 10 μL of primary nanobody (Nb_1) at a concentration of 10 μg mL^{-1} is applied to the electrode and incubated for 1 h at 37 °C, allowing the Nb_1 to bind to the streptavidin via the strep–biotin interaction. The electrode is then thoroughly washed with deionized water and DPBS (pH 7.4) to remove loosely bound Nb's and subsequently dried at room temperature. To block nonspecific binding and saturate any remaining biotin binding sites, a two-step blocking procedure is performed: The electrode is incubated with 1 % (*w/v*) BSA for 1 h at 4 °C to block nonspecific adsorption between the electrode and biomolecules. Then, 10 μL of biotin solution (0.5 mg mL^{-1}, ~2 mM in DPBS) is added and incubated for 30–60 min at room temperature to occupy any residual streptavidin sites. Following another DPBS wash, the immunosensor surface is exposed to varying concentrations of the target antigen (0–1000 pg mL^{-1}), drop-cast, and incubated for 1 h at 37 °C, allowing specific binding to the immobilized Nb_1. After removing unbound antigens by washing with DPBS, 10 μL of streptavidin-labelled $LiSmZrO_3$-Nb_2 bioconjugates is applied to the electrode and incubated for 1 h at 37 °C, completing the formation of the sandwich immunocomplex. Finally, the sensor is gently washed with 10 mM DPBS (pH 7.4) to eliminate any unbound conjugates. The fully assembled immunosensor is stored at 4 °C until further use.

2.6. Optimization and validation of the sandwich immunosensor for S1 detection

To achieve the most effective analytical performance of the fabricated immunosensor for S1 detection, different important experimental conditions were optimized by measuring the achieved currents using DPV and confirmed by SWV. For these experiments, 1000 pg mL^{-1} S1 was used in 10 mM Dulbecco's PBS (pH 7.4).

2.6.1. Optimization of nanobody concentrations

The selection of the best detector and capture probes for this procedure was carried out to optimize the performance of the immunosensor. We used three different serial concentrations (2.5, 5, and 10 μg mL^{-1}) of the Nb1-biotin (Nb_1) and Nb2-biotin (Nb_2).

2.6.2. Optimization of immunoreaction time

The time required for an effective immunocomplex to be formed between the nanobody and the antigen is crucial to the performance of the system. The selection of the best immunoreaction time between the capture probe (Nb_1) and the target antigen (S1) was performed to determine the most suitable time for optimal antigen-nanobody binding efficiency. We assessed the immunosensor at different times, ranging from 5 to 75 min with 15 min intervals.

2.6.3. Selectivity and cross-reactivity evaluation

To confirm the specificity of the immunosensor, cross-reactivity studies were conducted using potential interferent species, including glutamic acid, glutathione, L-tryptophan, and mouse serum protein (a complex mixture). Each interferent was tested individually at 10,000 pg mL^{-1} by incubating 10 μL on the sensor surface for 1 h. Additionally, a mixed solution containing S1 (1000 pg mL^{-1}) and all interferents (10,000 pg mL^{-1} each) was also evaluated. The immunosensor's response in these tests, using the previously optimized nanobody concentration and immunoreaction time, was compared to the specific target signal to confirm its selectivity and reliability for detecting the spike protein.

3. Results and discussion

3.1. Validation of the use of different labelled perovskite nanomaterials for secondary nanobody

The validation of the use of the perovskite material as a signal amplifier in the system is shown in Fig. S1. Perovskite nanomaterials possess many advantages as a material, such as being electrochemically stable, having enhanced ferroelectricity, and having high catalytic activity [28]. Therefore, it is expected that the coupling of this perovskite material to the detection nanobody (Nb_2) will result in an improved performance of the system. Furthermore, different approaches were assessed to analyse which specific modification of the Nb will give better results. Thus, three different approaches were used: (i) label-free, (ii) streptavidin-$LiSmZrO_3$, and (iii) cysteine-$LiSmZrO_3$. Based on the DPV and SWV results obtained in Fig. S1, it is evident that in the (ii) and (iii) approaches, the conjugation of the perovskite material to Nb_2 effectively increased the immunosensor's response toward S1 when compared to the label-free approach. Additionally, we can see that the streptavidin-labelled $LiSmZrO_3$ conjugation gave the highest signal. This is expected owing to the strong affinity that streptavidin has to the biotinylated Nb_2. Thus, we were able to confirm via electrochemical analysis that the presence of the perovskite nanomaterial served as a signal amplification, ultimately resulting in an improved current response of our immunosensor.

3.2. Electrochemical characterization of the step-by-step fabrication process of the sandwich immunosensor

Based on the morphological and electrochemical properties of the perovskite material reported by Monama and co-workers [20], $LiSmZrO_3$ has the potential to serve as an electroactive material in the construction of a sandwich-type biosensor. The fabrication steps are highlighted in Scheme 1. Streptavidin was first immobilized on the AuSPE surface via Au–SH interactions. The primary biotinylated nanobody (Nb_1), specific for the SARS-CoV-2 spike protein, was then effectively captured on the AuSPE||strep surface through the strong streptavidin–biotin affinity. To prevent nanobody degradation and block nonspecific adsorption, BSA was applied. Subsequently, the secondary nanobody (Nb_2), labelled with L-cysteine-$LiSmZrO_3$ via cross-linking chemistry, was immobilized onto the modified electrode surface. This configuration forms a sandwich-type nanobody-based immunosensor employing a perovskite material as the ECL label. The fabrication process and the interactions among the electrode, nanobodies, antigen,

and perovskite label were characterized using ECL measurements in 10 mM DPBS (pH 7.4) containing 50 μM $[Ru(bpy)_3]^{2+}$ and 100 mM TPA (Fig. 1). Additional characterization using CV, DPV, and SWV (Fig. S2a–c) further confirmed the successful construction of the sandwich immunosensor.

A similar immunosensing procedure was examined by January and co-workers [21], with CV, DPV, and SWV profiles of the sandwich immunosensor being extensively reported. Owing to the successful electrochemical analysis of the developed immunosensor, an ECL approach was used for this system. The ECL signals of each fabrication step are shown in Fig. 1. In Fig. 1, the electron transfer kinetics of the AuE||$[Ru(bpy)_3]^{2+}$/TPA system show a well-defined ECL signal. In the system, both the ruthenium complex and tripropylamine are electrochemically oxidized at the electrode surface. $[Ru(bpy)_3]^{2+}$ loses an electron to form $[Ru(bpy)_3]^{3+}$, while TPA is oxidized to TPA•$^+$, which rapidly undergoes deprotonation to generate a highly reducing radical species (TPA•). This radical then reduces $[Ru(bpy)_3]^{3+}$ back to $[Ru(bpy)_3]^{2+}$, but in its electronically excited state. The excited Ru complex subsequently relaxes to the ground state, emitting a photon in the process. The detected ECL signal, therefore, originates from this radiative decay of the excited $[Ru(bpy)_3]^{2+}$ with TPA acting as a co-reactant that enables the efficient generation of the luminescent species. This ECL signal was enhanced when streptavidin-thiol (strep) was deposited on the electrode. The unexpectedly high ECL intensity observed from strep can be attributed to several synergistic factors. Firstly, the strong Au—S bond formed by thiolated streptavidin ensures the formation of a dense and stable monolayer on the gold electrode, which facilitates efficient electron transfer necessary for the oxidation of $[Ru(bpy)_3]^{2+}$ to $[Ru(bpy)_3]^{3+}$, a key step in the ECL process [29]. Additionally, the proteinaceous nature of streptavidin may create a microenvironment that locally concentrates either the luminophore or TPA near the electrode surface via electrostatic or hydrogen bonding interactions, thus amplifying ECL output [30]. The streptavidin layer may also enhance the oxidation of TPA by reducing the required overpotential and promoting the generation of reactive TPA•$^+$ species [31]. Furthermore, the streptavidin coating can act as a protective barrier that minimizes quenching by preventing non-radiative decay pathways or access by interfering species, effectively increasing the ECL quantum yield [32]. Altogether, these surface, chemical, and electrochemical factors collectively explain the enhanced ECL signal in the presence of streptavidin-thiol. Then, after

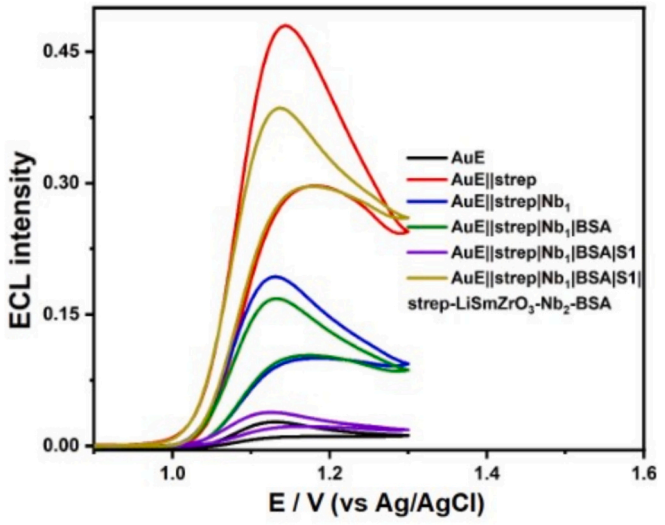

Fig. 1. Electrochemiluminescence profiles illustrating the stepwise fabrication of the sandwich-type immunosensor, which utilized 10 mM DPBS (pH 7.4) supplemented with 50 μM $[Ru(bpy)_3]^{2+}$ and 100 mM TPA. The data reflect the average of three independent replicates ($n = 3$), and baseline correction was applied to all recorded curves.

modification with Nb_1, there was a decrease in ECL signal, confirming the successful immobilization of the capture nanobody. This decrease can be attributed to several factors, such as Nbs can block active sites on the electrode, they can absorb or scatter the emitted light, lowering luminescence [33]. Similarly, Nbs can increase the distance between ECL labels and the electrode, which diminishes ECL efficiency, and they provide high coverage, which can cause steric hindrance, reducing label accessibility to the electrode [34]. Thereafter, the modified electrode was incubated in a blocking buffer (BSA) to block any inactive surface. The conductivity of the modified electrode was decreased, and the ECL signal was further reduced. Immediately after successive sandwich immune responses with S1, the ECL signal continued to decrease, highlighting the successful antigen-nanobody interaction. The interactions between the antigen and nanobodies can hinder the transfer of electrons between the electrode surface and the electrolyte. This reaction causes variations in the electrochemical signals [35]. Lastly, the electrode was incubated with the perovskite nanocomposite-bioconjugate (Nb_2), increasing the ECL signal. The enhancement arises from the perovskite nanomaterial label on Nb_2, which increases the ECL response through its unique photophysical properties and efficient electron transfer, combined with the dual-nanobody sandwich format that ensures non-competitive binding and higher antigen capture. This amplification is further supported by the $[Ru(bpy)_3]^{2+}$/TPA system, which provides a robust ECL signal [36,37]. All these results indicate that the proposed immunosensors have been successfully developed.

3.3. Electrochemical verification of the optimized parameters for the sandwich immunosensor

It is important to optimize the S1 binding time and dual nanobody concentration to find out which condition achieves the fastest detection and the best biosensing performance. Thus, to enhance the sandwich immunosensor's ability to detect the S1 antigen, a series of optimization experiments was conducted. Fig. S3a shows the relationship between the peak current signal and S1 concentration for the sandwich immunosensor. The current signal intensity was directly related to the concentration of the target analyte at the modified electrode, due to more electrons being transferred with increasing S1 concentration. Thus, based on the results obtained, 10 μg mL^{-1} S1 was selected as the optimized concentration. Then the intensity of the peak current response of the immunosensor was analyzed against the incubation time between the antigen-antibody complex for 75 min, with approximately 15 min intervals. Based on Fig. S3b, it is evident that there is a steady increase in the peak current response with an increase in the incubation time of S1, ranging from 5 to 60 min. Thereafter, we see a reduction in the signal. The current maximum was achieved for S1 with an incubation time of 60 min. Thus, the optimality of immunoreaction time was selected as 60 min. These results were all confirmed by a subsequent electrochemical technique shown in Fig. S4.

3.4. Immunosensor microscopic characteristics

The Scanning Electron Microscopy (SEM) and Energy Dispersive X-ray (EDX) analysis presented in Fig. 2 provide a comparative evaluation of the surface morphology and elemental composition of a bare AuSPE and the fully constructed immunosensor. In the SEM image of the bare AuSPE (Fig. 2a), the surface appears smooth and uniform with a fine granular texture typical of unmodified gold, serving as a reference for subsequent surface modifications. Correspondingly, its EDX spectrum (Fig. 2b) confirms an Au-dominant composition (72.03 % atomic concentration), with a small amount of oxygen likely due to environmental exposure or mild surface oxidation. In contrast, the SEM image of the immunosensor (Fig. 2c) reveals a highly heterogeneous surface with increased roughness and dense nanoparticle-like aggregates, indicative of successful biomolecular immobilization and nanomaterial integration. This transformation reflects the cumulative effect of layer-by-layer

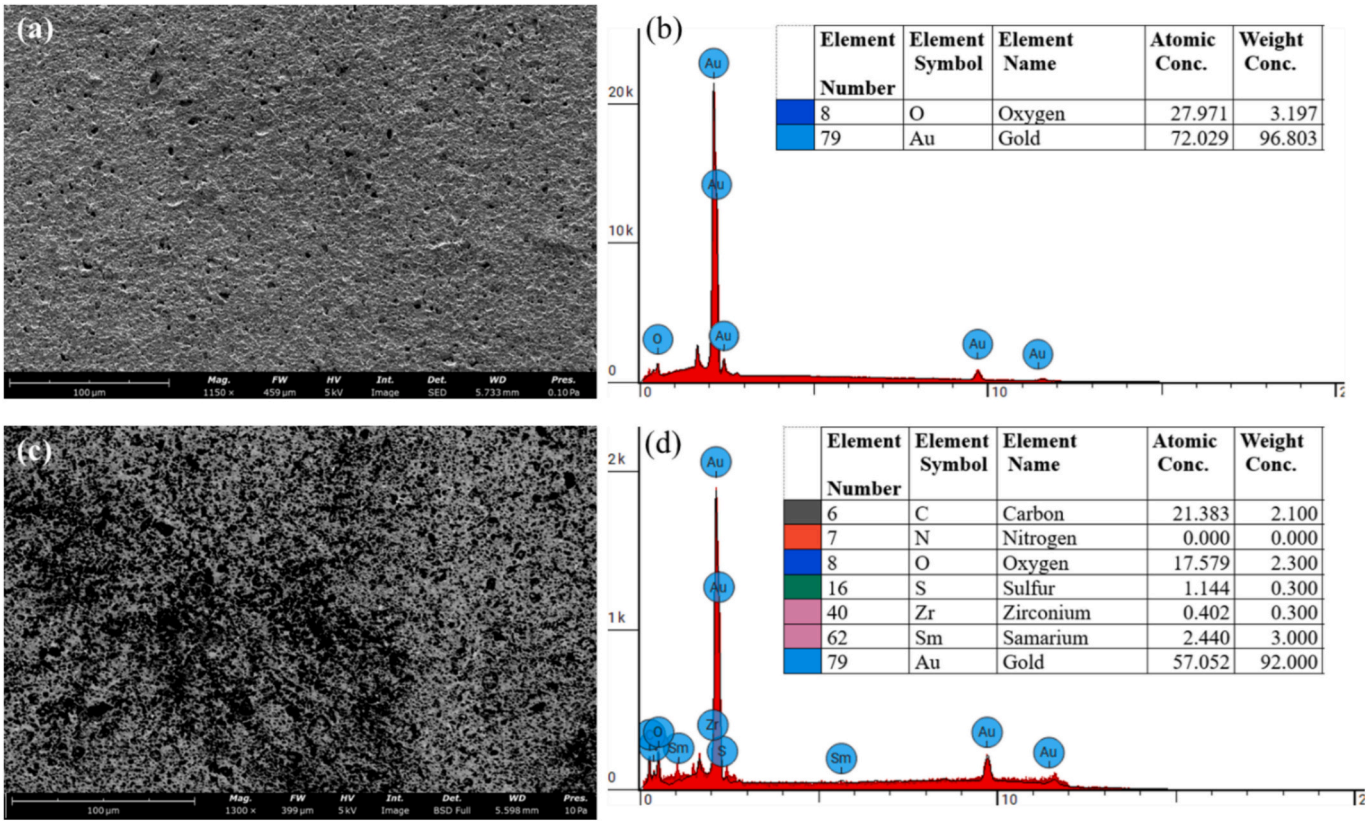

Fig. 2. The SEM micrographs at 100 μm of (a) bare AuSPE and (c) immunosensor AuSPE||strep|Nb_1|BSA|biotin|S1|strep-$LiSmZrO_3$-Nb_2 + BSA and their corresponding energy dispersive X-ray analysis (b) and (d).

modifications, including nanobody attachment and the deposition of the $LiSmZrO_3$ perovskite. The EDX analysis of the immunosensor (Fig. 2d) supports this, showing a more complex elemental profile with the presence of carbon, oxygen, sulfur, zirconium, and samarium, which are attributed to the biological components and perovskite nanomaterial. The reduction in gold signal (to 57.05 % atomic concentration) further confirms the effective coverage of the Au surface. Collectively, these results validate the successful fabrication of the immunosensor through both morphological and compositional evidence.

3.5. *Electrochemical properties of the immunosensor (AuSPE||strep|Nb_1|BSA|biotin|S1|strep-$LiSmZrO_3$-Nb_2 + BSA)*

3.5.1. *Sandwich immunosensor scan rate studies*

CV techniques were employed to investigate the chemical kinetics of S1 on the modified surface electrode (AuSPE||strep|Nb_1|BSA|biotin|strep-$LiSmZrO_3$-Nb_2 + BSA), in 10 mM DPBS, pH 7.4, at different scan rates ranging between 10 and 100 mV/s. Based on this, a Randles–Ševčík plot of redox peak current (Ip) vs. the square root of scan rate ($v^{1/2}$) was obtained as shown in Fig. S2d. The results confirm the validity of the sandwich immunosensor for detecting S1, as evidenced by the linear relationship between I_{pa} and I_{pc} and the square root of $v^{1/2}$ and the increased separation between redox peaks, indicating that electron transfer is influenced by the diffusion of electroactive species. The anodic peak at approximately +1.0 V (A) corresponds to the oxidation of gold to surface oxides. Although this process is typically surface-controlled on bare gold electrodes, the observed $v^{1/2}$ dependence suggests mixed kinetic–diffusion behavior arising from ion and charge redistribution within the modified electrode interface. The multilayered surface architecture, comprising streptavidin, nanobody, antigen, and perovskite nanocomposite components, introduces porous and heterogeneous domains that facilitate the movement of electrolyte ions and redox species through interfacial films and nanocomposite pores. Thus, the overall current response reflects a combination of surface-confined gold oxidation and diffusional processes within the modified film, highlighting the complex interplay between interfacial charge transfer, ion mobility, and the electroactive structure of the sensing interface.

3.5.2. *Detection of S1 in physiological buffer*

Under optimized conditions, the analytical performance of the sandwich electrochemical immunosensor was assessed by evaluating the peak current response at various concentrations of the S1 antigen. Fig. 3 shows the ECL curves and their corresponding calibration curves. The y-axis in the calibration plot represents the adjustment of the curve that subtracts the signal of the biosensor and the signal from incorporating the S1 antigen from one another. The labelled nanobody-based sandwich immunosensor achieved the sensitive determination for S1, which can be attributed to the following three reasons: (i) the introduction of the perovskite material influences the electrochemical activity of the system leading to superior conductivity; (ii) biotinylated-Nb can facilitate the strong immobilization with AuSPE||strep to form a gold-thiolate-biotin Nb bond and with Nb–perovskite nanomaterial conjugates (Nb_2); and (iii) the Nb has a high affinity for S1 which triggers an immunological reaction resulting in the formation of an immunocomplex at the sensing interface. In Fig. 3, the ECL signal gradually increased as the S1 concentration increased from 0 to 1000 pg mL^{-1}. Thus, the ECL intensity and the target analytes' concentration had a very good linear relationship. The gradual increase in the ECL signal with the concentration of the target analytes is due to the nature of the ECL reaction. In ECL, the analyte interacts with the luminophore or co-reactants at the electrode surface. As the concentration of the analyte increases, more molecules are available to participate in the electrochemical reactions, leading to a higher production of excited states that emit photons [38,39]. This results in a stronger ECL signal. Additionally, the

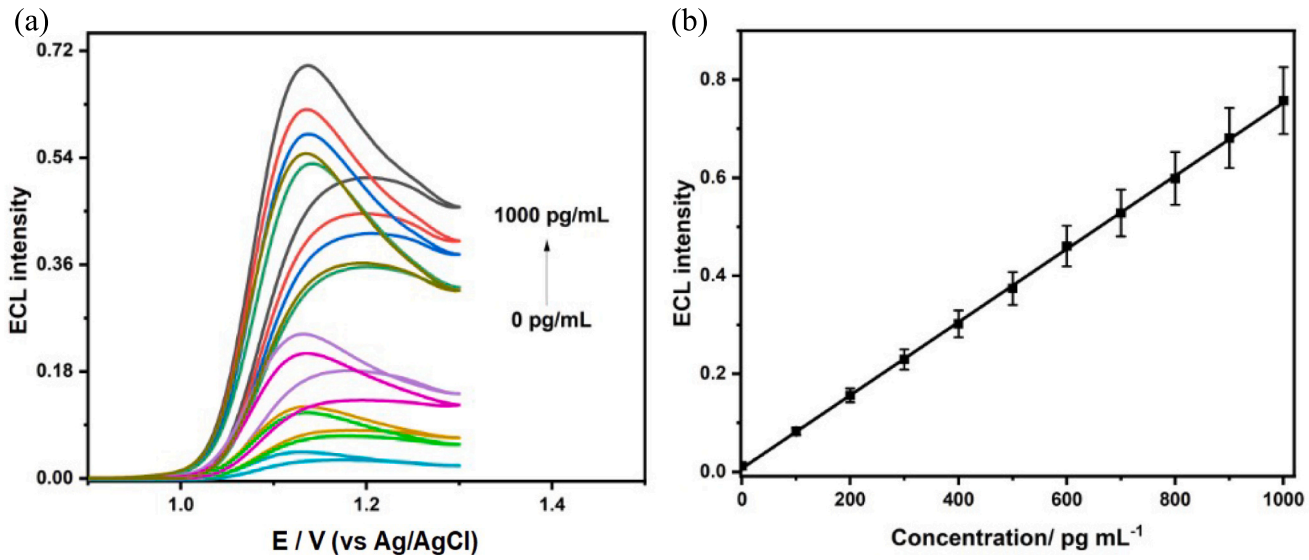

Fig. 3. Conventional ECL generated for the sandwich nanobody-based immunosensor and its (b) corresponding calibration plot for triplicate analysis ($n = 3$) in 10 mM DPBS containing 50 μM $[Ru(bpy)_3]^{2+}$ and 100 mM TPA.

relationship between the analyte concentration and the ECL signal is often linear within a certain range, making it a valuable tool for quantitative analysis in biosensing and diagnostics. Thereafter, using the limit of detection (LOD) = 3σ / k and limit of quantification (LOQ) = 10σ /k, the values of 0.04 and 0.121 pg mL^{-1} for ECL were obtained, respectively.

Furthermore, the linear regression equation for the S1-sensitive immunosensor in DPBS was ECL intensity (I) = 0.00074× C (pg mL^{-1}) + 0.0122, and the R-squared correlation coefficient (R^2) was 0.9989. Based on its established linear calibration curve, the applicability of the developed immunosensor for detecting the spike protein was evaluated using human serum samples.

3.5.3. *Detection of S1 in real sample*

To confirm the validity of the immunosensor in this environment, the immunosensor was evaluated in a real sample (human serum), as shown in Fig. 4. For the detection, the sample was diluted 1:10 in 10 mM DPBS. Using the aforementioned LOD and LOQ equations, the following results were obtained: 0.38 and 1.15 pg mL^{-1}, respectively. The analytical performance of the developed immunosensor, summarized in Table S1, shows higher sensitivity and lower LOD and LOQ values in DPBS compared to human serum. This is expected, as physiological buffers like DPBS provide a cleaner environment that promotes efficient interaction between the target analyte and the sensor surface. In contrast, human serum is a complex biological fluid containing various proteins, enzymes, and other interfering substances that can interact with the immunosensor, potentially blocking binding sites, causing nonspecific adsorption, or fouling the electrode surface. These effects can impair the sensor's performance and reduce its sensitivity, supporting previous findings that buffer systems are more favorable for optimal immunosensor function. The obtained analytical characteristics demonstrate that the developed Nb-based sandwich immunosensor can be used to determine the S1 concentration to be tested, as well as its accuracy and success in detecting the virus protein, making it an ideal platform for

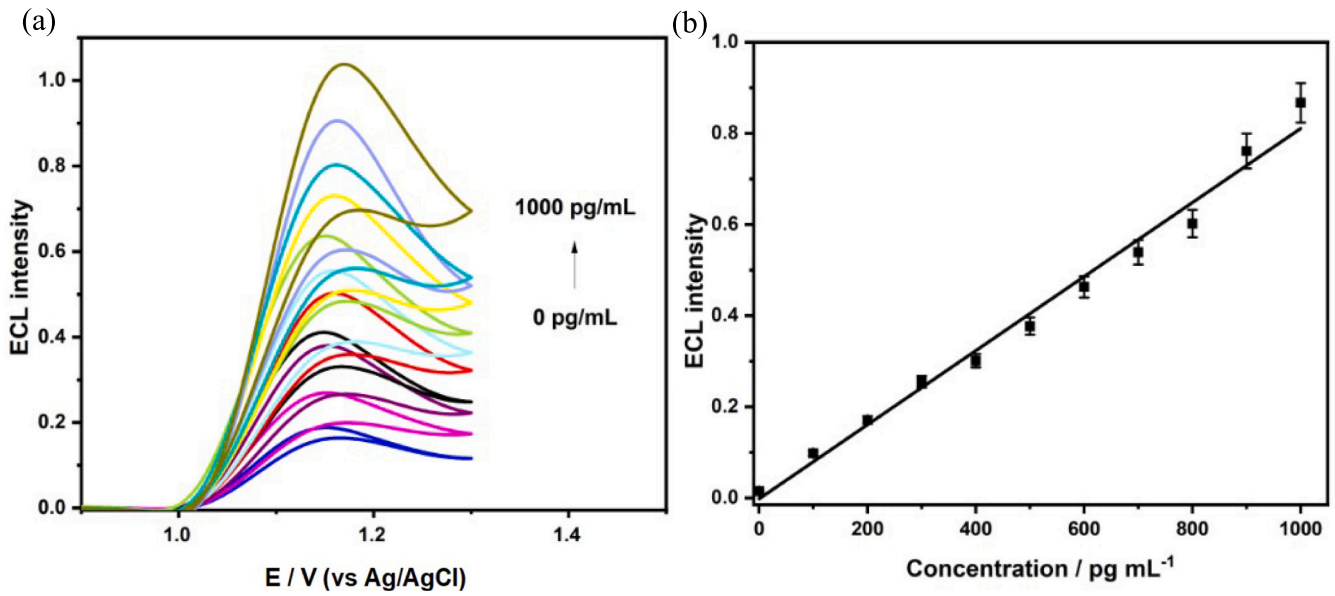

Fig. 4. Conventional ECL generated for the sandwich nanobody-based immunosensor and its (b) corresponding calibration plot for triplicate analysis (n = 3) in 10 % human serum containing 50 μM $[Ru(bpy)_3]^{2+}$ and 100 mM TPA.

assessing the presence of the virus.

3.5.4. Comparative studies

This work reports, for the first time, the development of an electrochemiluminescent sandwich-type Nb-based immunosensor incorporating a perovskite nanomaterial label for the sensitive and selective detection of the SARS-CoV-2S protein. In Table 1, it is evident that only one other nanobody-based immunosensor has been reported for the detection of S1 protein; however, that platform achieved a slightly higher sensitivity (LOD = 5×10^{-3} pg mL^{-1}) using a PEC system with a single nanobody. In contrast, our ECL immunosensor attained an LOD of 0.04 pg mL^{-1}, which, although marginally higher, was achieved under a more complex sandwich configuration incorporating dual nanobodies and a perovskite nanomaterial label, representing a distinctly different transduction and recognition strategy. The modest numerical difference is outweighed by the conceptual advance of combining two nanobodies recognizing distinct S1 epitopes with a novel perovskite-based ECL amplifier, producing a robust and reproducible sensing interface that remains highly competitive with the lowest reported values for S1 protein. Table 1 also summarizes several nanobody-based sandwich immunosensors for other biomarkers, many of which achieved picogram- to femtogram-level sensitivities depending on analyte size and detection modality. Our platform achieved one of the lowest detection limits reported for a large viral antigen (≈30 kDa), emphasizing that molecular-weight-related diffusion and steric constraints can be effectively mitigated through rational nanobody pairing and nanoscale interface design.

Importantly, the current work represents the first reported dual-nanobody, perovskite-labelled ECL immunosensor for SARS-CoV-2S1, marking a significant step forward in nanobody-based viral diagnostics. Literature reports indicate that single-nanobody systems typically achieve LODs around 0.1 ng mL^{-1} [30]; in comparison, our design demonstrates a roughly 2500-fold improvement in sensitivity, achieved without reliance on conventional antibody chemistry. The use of a $LiSmZrO_3$ perovskite nanomaterial as an ECL label enhanced luminophore–co-reactant electron transfer and photonic efficiency, further contributing to the high signal-to-noise ratio.

When compared with other ECL SARS-CoV-2S1 and S1-RBD biosensors, our immunosensor achieved a sensitivity comparable to or better than most reported systems, despite the differences in material composition and transduction method. To date, only two ECL biosensors have been reported for S1-RBD detection. Although one achieved a lower LOD [48] than ours, it relied on high-surface-area nanomaterials (such as CNDs and AuNPs) and strong luminophores integrated with

Table 1
Comparative performance of nanobody-based, electrochemiluminescence, and electrochemical SARS-CoV-2 immunosensors, and commercial ELISA kits.

Electrode modification	Biomarker	Technique	Linear range (pg mL^{-1})	LOD (pg mL^{-1})	Protein MW (kDa)	Ref.
Nanobody-based electrochemical immunosensors						
ITO|| Au@TiO_2|Nb|BSA|SP	SARS-CoV-2SP	PEC	0.015–15,000	5×10^{-3}	76.9	[25]
SPCE||Au|PVA|CA NFM|AuNPs	Parathion	EIS	1.5–6400 × 10^3	0.48	0.29126	[33]
AuSPE||cysteamine|GA|Nb	*H. pylori*	DPV	10,000–1000 × 10^3	5.9 × 10^3	7.1	[34]
SPCE||PVA|G-AuNPs NFM|SCP|GA	Quinalphos	EIS	60–1000 × 10^3	50.74	0.2983	[43]
SPCE||PVA|PAA NFM| 19-NT-OVA BSA|Nb_2F7-HRP	19-NT	CV	6–100 × 10^3	2.14	0.2744	[44]
GCE|| AuNPs@ZIF-8 @MWCNTs| A1-C4bpα	AFP	DPV	0.1–1 × 10^5	0.033	63	[45]
GCE|| rGO@AuNPs|Nb_1|BSA|PSA|Nb_2-SBP-HRP	PSA	DPV	100–100 × 10^3	80	34	[46]
GCE||GO-PB-PTCNH$_2$|AuNPs|Nb|BSA| AFB_1	AFB_1	DPV	10–100 × 10^3	3.3	0.312277	[47]
GCE||strep|biotin-Nb_1|Cry1Ab|HRP-Nb_2-PAn	Cry1Ab	DPV	100–1000 × 10^3	70	130	[40]
GCE||T-COF|Nb|TSLP-Ag^+	TSLP	ECL	1–4 × 10^3	2.72	23	[25]
GCE||GR-GS|Nb_1|BSA|PCT|CdTe@SiO_Nb_2	PCT	ECL	10–20 × 10^3	3.4	13	[41]
GCE||Nafion|$CaCO_3$|Au|Ru(bpy)$_3^{2+}$|Nb|BSA| OTA	OTA	ECL	10–100 × 10^3	5.7	0.404	[42]
Electrochemiluminescence SARS-CoV-2S1 biosensors						
SPE||CNDs	S1	ECL	7.5 × 10^{-7}–7.5 × 10^{-3}	7.5 × 10^{-7}	180	[48]
SPE||AuNPS|luminol	S1	ECL	1–100,000	1.0	180	[49]
GCE||P-MOGs-Ab_1|NP|Ab_2-Au@Cu_2O@Fe_3O_4	NP	ECL	0.01 – 100,000	1.5 × 10^{-3}	114	[50]
ITO||Ru@bp-SNA	SARS-CoV-2 IgG	ECL	5–1000,000	2.9	150	[51]
GCE||DMSN@CdSe|ZnSQDs	NP	ECL	5–50,000	3.33	114	[52]
ITO||CoO@N-C	NP	ECL	0.008–4000	1.6 × 10^{-3}	114	[53]
Electrochemical SARS-CoV-2S1-RBD immunosensors						
ITO||C-NC|Ab_1|BSA|S1-RBD|Ab_2	S1-RBD	EIS	0.0012–120	5.8 × 10^{-4}	25	[54]
ITO||GNPs@MUA|Ab_1|BSA|S1-RBD|Ab_2	S1-RBD	EIS	0.002–100	5.7 × 10^{-4}	25	[55]
SPCE||Ab_1|BSA|S1|HRP-Ab_2	S1	Chronoamperometry	500–10,000	130	180	[56]
SPCE||SiO_2@UiO-66|Ab	S1	EIS	0.1–10,000	0.1	180	[57]
Graphite electrode||ACE2 peptide-mimic|Ab	RBD S1	EIS	167–994	45.08	25	[58]
SPCE||Ni(OH)$_2$|Ab	S1	DPV	0.001–1000,000	3 × 10^{-4}	180	[59]
SARS-CoV-2S1-RBD ELISA assays						
–	SARS-CoV-2S1-RBD	ELISA	6.14–1500	4.5	30	ThermoFisher
–		ELISA	390–25,000	90	30	Elabscience
–		ELISA	630–40,000	140	30	BioLegend
AuSPE||strep|Nb_1|BSA|S1|strep-$LiSmZrO_3$-Nb_2-BSA	SARS-CoV-2S1-RBD	ECL (DPBS) ECL (human serum)	100–1000	0.04 0.38	30	This work

Gold nanoparticles (AuNPs), horseradish peroxidase (HRP), two-dimensional (2D) metal-organic framework (MOF), interdigitated electrode (IDE), carbon cloth (CC), differential pulse voltammetry (DPV), chronopotentiometry (CP), electrochemical impedance spectroscopy (EIS), magnetic beads (MBs), spike protein (SP), Nucleocapsid protein (N), redox probe = Fc-R-COOH; R = -CONH- C_6H_4-NHOC-$(CH_2)_2$-, tetramethyl benzidine (TMB), gold nanoparticles-capped 11-mercaptoundecanoic acid (GNPs@MUA), indium tin oxide (ITO), conducting nanocomposite (C-NC), chronoamperometry (CA), bismuth tungstate/bismuth sulfide composite (Bi_2WO_6/Bi_2S_3), graphitic carbon nitride sheet decorated with gold nanoparticles (AuNPs) and tungsten trioxide sphere composite (g-C_3N_4/Au/WO_3), localized surface plasmon resonance (LSPR), photoelectrochemical (PEC), thymic stromal lymphopoietin (TSLP), tetrakis(4-aminophenyl)ethene- derived covalent organic frameworks (T-COF), human procalcitonin (PCT), chitosan–graphene nanocomposite (GR–CS), ochratoxin A (OTA), carbon nanodots (CNDs), conducting nanocomposite (C-NC), gold nanoparticles capped with 11-mercaptoundecanoic acid (GNPs@MUA), silica-coated with the metal-organic framework UiO-66 (SiO_2@UiO-66), nickel hydroxide nanoparticles (Ni(OH)$_2$, nucleocapsid protein (NP), metal–organic gels (MOGs), bipolar silica nanochannel array (bp-SNA), dendritic mesoporous silica nanospheres loaded with CdSe/ZnS quantum dots (DMSN@QDs), magnetic N-doped carbon (CoO@N-C).

antibody-based capture systems, rather than our dual-nanobody mixed immobilization strategy. This distinction highlights that their enhanced sensitivity likely stems from material and luminophore effects. Thus, in contrast, our platform introduces perovskite nanomaterials as labels in an Nb-based S1 sensor for the first time; these labels have distinct photophysical properties that have not yet been fully optimized for maximum ECL efficiency. Table 1 also summarizes electrochemical S1-RBD immunosensors, most of which employ impedimetric or amperometric detection. Among these, only two are sandwich-type configurations, both based on electrochemical impedance spectroscopy (EIS), with exceptionally low LODs of 5.7×10^{-4} pg mL^{-1} and 5.8×10^{-4} pg mL^{-1}. These ultralow values can be attributed to the intrinsic sensitivity of EIS toward interfacial charge transfer changes at the electrode surface, coupled with the use of highly conductive nanostructured interfaces such as C-NC and AuNPs@MUA that maximize electron transfer and analyte binding efficiency. In contrast, our dual-nanobody ECL sandwich-type immunosensor, though operating via a different transduction mechanism, achieved a comparable LOD. When comparing sandwich-type electrochemical biosensors with non-sandwich configurations, it becomes evident that the sandwich format markedly enhances detection performance by enabling bivalency analyte recognition and improved target capture. Although EIS platforms attain lower LODs through optimized nanomaterial interfaces and well-established antibody chemistry, our dual-nanobody ECL system introduces a novel perovskite-based transduction strategy that offers high specificity, photostability, and potential for multiplexed detection. Additionally, the reported immunosensor achieved a comparable or lower LOD than commercial SARS-CoV-2 RBD ELISA kits (e.g., Thermo Fisher 4.5 pg mL^{-1}; Elabscience 90 pg mL^{-1}; BioLegend 140 pg mL^{-1}), shows practical applicability, and offers a pathway for non-antibody-based, high-affinity, and potentially more stable recognition elements for SARS-CoV-2 diagnostics. The table reveals that only three nanobody-based immunosensors employing electrochemiluminescence have been reported to date, all of which target biomarkers other than the S1 antigen. The complete absence of S1-specific electrochemiluminescent nanobody platforms in the literature underscores the originality and potential impact of the present work, which addresses this critical gap for the first time.

3.5.5. Control studies to confirm the electrochemical analysis of the immunosensor

Control experiments using SWV and DPV analysis were performed to validate the electrochemical properties of the developed sandwich nanobody-based immunosensor. This was achieved by developing several electrochemical immunosensors in the absence of the Nb_1, strep, and the antigen (S1), and was compared to the bare electrode and the complete modified electrode (immunosensor). These results are shown in Fig. S5, which highlights that in the absence of any of the steps, there will be a significant impact on the response of the system. In the figure, control samples (i) to (iii) show an increase in the peak current response when compared to the bare, which shows that we now have efficient interactions occurring on the surface of the electrode. Then we see that the immunosensor (iv) showed the lowest peak current response, confirming that antigen-antibody immunocomplexes were effectively formed and that each step is crucial to the successful fabrication of the immunosensor. It also highlights that the primary and secondary Nb's exhibited selective recognition of the spike protein. This was further highlighted via DPV in Fig. S6.

3.5.6. Selectivity, reproducibility, and stability studies

High-sensitivity and reliable biosensors need to have excellent specificity. Apart from the target analyte, some proteins may also interact with the immune substrate on the surface of the electrode. Thus, to confirm the selectivity of the AuSPE||strep|Nb_1|BSA|biotin|S1|strep-$LiSmZrO_3$-Nb_2 + BSA electrode to S1, the immunosensor was tested by incubating the target S1 (1000 pg mL^{-1}) against several inferring substances (1×10^4 pg mL^{-1}) such as (i) glutamic acid (G.acid), (ii) glutathione (GSH), (iii) tryptophan (Trp), (iv) mouse IgG, and a (v) mix of all the interferents with the target analyte (S1). The results of the study in Fig. 5a revealed that the immunosensor's response was significantly different when it came to the specific and non-specific antigens. For the non-specific antigens, the response was higher because there was no binding, which allowed the maximum number of nanobodies to bind to the electrode, showing that non-specific absorption occurred. On the other hand, when the target protein was placed on the electrode at a lower concentration, it exhibited strong interactions, as shown by the significant decrease in current response. This was similarly seen in the mixture (non-specific and specific antigens). However, in the figure, it is evident that the mouse IgG sample had the greatest influence on the current response of the electrode surface among the other interferents. This is expected because the mouse IgG sample used contained a significant number of proteins, which ultimately could've bound to the surface of the modified electrode. Nonetheless, the results of the study revealed that the sandwich-type immunosensor made using the two Nbs had good selectivity and specificity toward the target analyte.

The peak current response of AuSPE||strep|Nb_1|BSA|biotin|S1|strep-$LiSmZrO_3$-Nb_2 + BSA electrode with concentrations of 1000 pg mL^{-1} S1 stored in the dark at 4 °C for 25 days was tested. After the long-term storage, the immunosensor possessed less signal attenuation with a retained signal of more than 85 % after 25 days, as shown in Fig. 5b, indicating the exceptional stability of this fabricated sensor. This was further confirmed via SWV in Fig. S7.

4. Conclusion

To summarize, we successfully developed a highly sensitive and selective electrochemiluminescent immunosensor for the detection of the spike (S1) protein, which is emerging as a critical biomarker for identifying and monitoring PVRs. Detecting the presence of residual viral antigens like the S1 protein is vital for assessing ongoing infection risk and understanding viral persistence mechanisms. The proposed immunosensor employed a perovskite-labelled nanobody-based sandwich configuration, where nanobody pairs (Nb1RBDnoCys as capture Nb and Nb2RBDNoCys as detection Nb) provide exceptional specificity toward the S1 antigen. The integration of perovskite nanoparticles amplifies the electrochemical signal, resulting in superior analytical performance suitable for point-of-care monitoring of PVRs. The electrochemiluminescent immunosensor achieved a LOD of 0.04 pg mL^{-1}, demonstrating excellent sensitivity and comparable analytical performance. The biosensor did not show cross-reactivity with antigens such as glutamic acid, glutathione, tryptophan, and mouse IgG protein, implying high selectivity of the method, and was still shown to be functional after storage at 4 °C for 25 days. To further enhance the sensitivity, signal stability, and simplify the assay protocol, future designs could benefit from directly coupling the detection nanobody (Nb_2) to horseradish peroxidase (HRP). This strategy would eliminate the need for intermediate signal amplification steps involving perovskite particles, reduce background interference, and streamline fabrication. Moreover, HRP-Nb_2 conjugates may improve reproducibility and facilitate broader clinical application by enabling a more robust, single-step enzymatic signal transduction mechanism. Such optimization could pave the way for the development of next-generation immunosensors for rapid and accurate viral antigen detection.

CRediT authorship contribution statement

Jaymi January: Writing – original draft, Visualization, Methodology, Investigation. **Olivier Zwaenepoel:** Validation, Resources. **Nelia Sanga:** Validation. **Jan Gettemans:** Writing – review & editing, Supervision, Resources. **Emmanuel Iwuoha:** Writing – review & editing, Supervision, Project administration, Funding acquisition, Conceptualization.

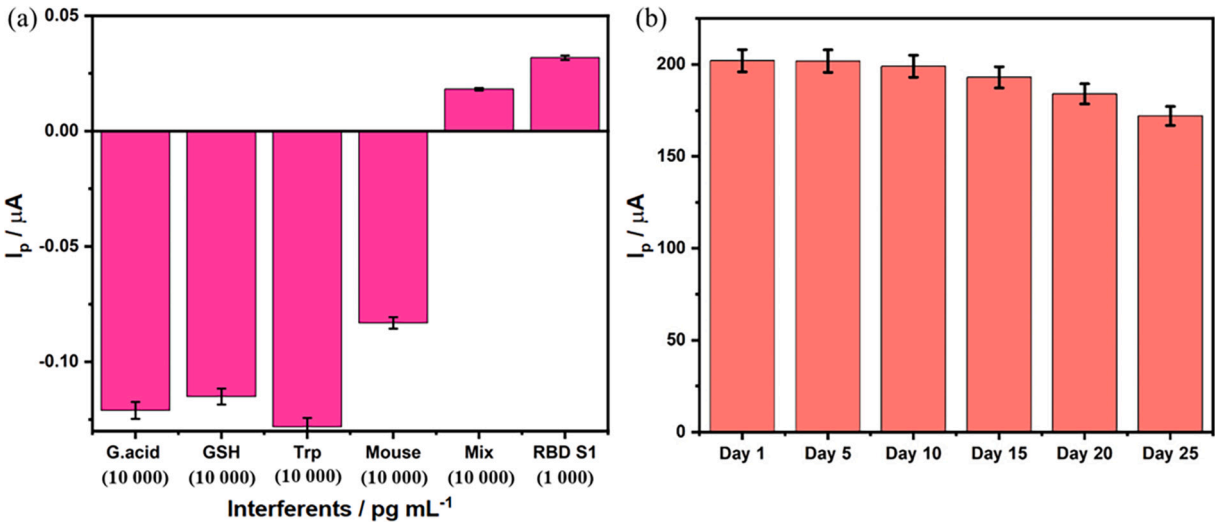

Fig. 5. (a) Interference studies based on electrochemical analysis obtained in the presence of 1000 pg mL^{-1} S1 and 10-fold interferents (1×10^4 pg mL^{-1}). (b) Electrochemical response via SWV of the developed immunosensor (AuSPE||strep|Nb_1|BSA|biotin|S1|strep-LiSmZrO$_3$-Nb_2 + BSA), after storing at 4 °C for 25 days. Experiments were performed in triplicate ($n = 3$).

Funding

This study received financial support from the National Research Foundation (NRF) of South Africa through several grants: (i) a Doctoral Scholarship (Ref: MND210414594777); (ii) the SARChI Chair in Nano-Electrochemistry and Sensor Technology (Ref: SARC20130101-085102); (iii) the South African NRF-Belgian BELSPO Joint Research Programme grant for the LUMIPLAT project (Ref: BELSP22091056954); and (iv) Research Programme grant GOA 01G00824.

Declaration of competing interest

The authors declare the following financial interests/personal relationships which may be considered as potential competing interests: Jaymi January reports financial support was provided by SA (NRF)-Belgium (BELSPO) Joint Research Programme Grant. If there are other authors, they declare that they have no known competing financial interests or personal relationships that could have appeared to influence the work reported in this paper.

Acknowledgements

All experimental work was carried out utilizing the resources at SensorLab, University of the Western Cape, and the Nanobody Lab at Ghent University. The authors sincerely thank Gobeng Release Monama for the synthesis of the LiSmZrO$_3$ perovskite nanomaterial, which was essential for modifying the secondary nanobody.

Appendix A. Supplementary data

Supplementary data to this article can be found online at https://doi.org/10.1016/j.bioelechem.2025.109137.

Data availability

Data will be made available on request.

References

[1] N.A. El-Baky, A.A. Amara, V.N. Uversky, E.M. Redwan, Intrinsic factors behind long COVID: III. Persistence of SARS-CoV-2 and its components, J. Cell. Biochem. 125 (2024) e30514, https://doi.org/10.1002/jcb.30514.

[2] G. Gupta, D. Buonsenso, J. Wood, S. Mohandas, D. Warburton, Mechanistic insights into long COVID: viral persistence, immune dysregulation, and multi-organ dysfunction, Compr. Physiol. 15 (2025) e70019, https://doi.org/10.1002/cph4.70019.

[3] H.M. Machkovech, A.M. Hahn, J. Garonzik Wang, N.D. Grubaugh, P.J. Halfmann, M.C. Johnson, J.E. Lemieux, D.H. O'Connor, A. Piantadosi, W. Wei, T.C. Friedrich, Persistent SARS-CoV-2 infection: significance and implications, Lancet Infect. Dis. 24 (2024) e453–e462, https://doi.org/10.1016/S1473-3099(23)00815-0.

[4] J. Goode, G. Dillon, P.A. Millner, The development and optimisation of nanobody based electrochemical immunosensors for IgG, Sens. Actuat. B: Chem. 234 (2016) 478–484, https://doi.org/10.1016/j.snb.2016.04.132.

[5] S. Pirkalkhoran, W.R. Grabowska, H.H. Kashkoli, R. Mirhassani, D. Guiliano, C. Dolphin, H. Khalili, Bioengineering of antibody fragments: challenges and opportunities, Bioengineering 10 (2023) 122, https://doi.org/10.3390/bioengineering10020122.

[6] M. Kijanka, F.J. Warnders, M. El Khattabi, M. Lub-De Hooge, G.M. Van Dam, V. Ntziachristos, L. De Vries, S. Oliveira, P.M.P. Van Bergen En Henegouwen, Rapid optical imaging of human breast tumour xenografts using anti-HER2 VHHs site-directly conjugated to IRDye 800CW for image-guided surgery, Eur. J. Nucl. Med. Mol. Imaging 40 (2013) 1718–1729, https://doi.org/10.1007/s00259-013-2471-2.

[7] L. Li, X. Liu, S. He, H. Cao, B. Su, T. Huang, Q. Chen, M. Liu, D.P. Yang, Electrochemiluminescence immunosensor based on nanobody and Au/CaCO$_3$ synthesized using waste eggshells for ultrasensitive detection of ochratoxin A, ACS Omega 6 (2021) 30148–30156, https://doi.org/10.1021/acsomega.1c05213.

[8] J.P. Salvador, L. Vilaplana, M.P. Marco, Nanobody: outstanding features for diagnostic and therapeutic applications, Anal. Bioanal. Chem. 411 (2019) 1703–1713, https://doi.org/10.1007/s00216-019-01633-4.

[9] T.S. Pillay, S. Muyldermans, Application of single-domain antibodies ("Nanobodies") to Laboratory Diagnosis, Ann. Lab. Med. 41 (2021) 549–558, https://doi.org/10.3343/alm.2021.41.6.549.

[10] S. Lara, A. Perez-Potti, Applications of nanomaterials for immunosensing, Biosensors 8 (2018) 104, https://doi.org/10.3390/bios8040104.

[11] N.J. Ronkainen, S.L. Okon, Nanomaterial-based electrochemical immunosensors for clinically significant biomarkers, Materials 7 (2014) 4669–4709, https://doi.org/10.3390/ma7064669.

[12] H. Ju, X. Zhang, J. Wang, Nanomaterials for immunosensors and immunoassays, in: Biological and Medical Physics, Biomedical Engineering, 2011, pp. 425–452, https://doi.org/10.1007/978-1-4419-9622-0_15.

[13] J.F. Rusling, Nanomaterials-based electrochemical immunosensors for proteins, Chem. Rec. 12 (2012) 164–176, https://doi.org/10.1002/tcr.201100034.

[14] Y. Lai, L. Wang, Y. Liu, G. Yang, C. Tang, Y. Deng, S. Li, Immunosensors based on nanomaterials for detection of tumor markers, J. Biomed. Nanotechnol. 14 (2018) 44–65, https://doi.org/10.1166/jbn.2018.2505.

[15] J. Ezzati Nazhad Dolatabadi, M. De La Guardia, Nanomaterial-based electrochemical immunosensors as advanced diagnostic tools, Anal, Methods 6 (2014) 3891–3900, https://doi.org/10.1039/c3ay41749b.

[16] M. Pan, Y. Gu, Y. Yun, M. Li, X. Jin, S. Wang, Nanomaterials for electrochemical immunosensing, Sensors 17 (2017) 1041, https://doi.org/10.3390/s17051041.

[17] W. Wang, Q. Wang, H. Xie, D. Wu, N. Gan, A universal assay strategy for sensitive and simultaneous quantitation of multiplex tumor markers based on the stirring rod-immobilized DNA-LaMnO$_3$ perovskite-metal ions encoded probes, Talanta 222 (2021) 121456, https://doi.org/10.1016/j.talanta.2020.121456.

[18] Z. Yu, J. Xu, Y. Li, H. Gong, Q. Wei, D. Tang, Ferroelectric perovskite-enhanced photoelectrochemical immunoassay with the photoexcited charge-transfer of a

built-in electric field, J. Mater. Chem. C: Mater. 9 (2021) 14351–14358, https://doi.org/10.1039/D1TC03097C.
[19] J. January, M. Oranzie, K.C. Januarie, G.R. Monama, N.A. Sanga, Z. Leve, C. Cupido, K.D. Modibane, O.V. Uhuo, E. Iwuoha, A novel $LiSmZrO_3$ perovskite-amplified interferon gamma-sensitive electrochemical tuberculosis aptasensor, Next Res. 2 (2025) 100093, https://doi.org/10.1016/j.nexres.2024.100093.
[20] G.R. Monama, M.E. Ramoroka, K.E. Ramohlola, M.W. Seleka, E.I. Iwuoha, K. D. Modibane, Terbium- and samarium-doped Li_2ZrO_3 perovskite materials as efficient and stable electrocatalysts for alkaline hydrogen evolution reactions, Environ. Sci. Pollut. Res. (2024), https://doi.org/10.1007/s11356-024-34846-x.
[21] J. January, O. Zwaenepoel, J. Gettemans, E. Iwuoha, Highly sensitive nanobody-immunosensor for macrophage-capping protein, Biosens. Bioelectron. 287 (2025) 117681, https://doi.org/10.1016/j.bios.2025.117681.
[22] S. Maher, M. Kamel, Z. Demerdash, H. El Baz, O. Sayyouh, A. Saad, N. Ali, F. Salah, S. Atta, Gold conjugated nanobodies in a signal-enhanced lateral flow test strip for rapid detection of SARS-CoV-2S1 antigen in saliva samples, Sci. Rep. 13 (2023) 10643, https://doi.org/10.1038/s41598-023-37347-y.
[23] Y. He, Z. Xu, T. Kasputis, X. Zhao, I. Ibañez, F. Pavan, M. Bok, J.P. Malito, V. Parreno, L. Yuan, R.C. Wright, J. Chen, Development of nanobody-displayed whole-cell biosensors for the colorimetric detection of SARS-CoV-2, ACS Appl. Mater. Interfaces 15 (2023) 37184–37192, https://doi.org/10.1021/acsami.3c05900.
[24] M. Kamel, S. Maher, H. El-Baz, F. Salah, O. Sayyouh, Z. Demerdash, Non-invasive detection of SARS-CoV-2 antigen in saliva versus nasopharyngeal swabs using nanobodies conjugated gold nanoparticles, Trop. Med. Infect. Dis. 7 (2022) 102, https://doi.org/10.3390/tropicalmed7060102.
[25] Y. Chen, W. Duan, L. Xu, G. Li, Y. Wan, H. Li, Nanobody-based label-free photoelectrochemical immunoassay for highly sensitive detection of SARS-CoV-2 spike protein, Anal. Chim. Acta 1211 (2022) 339904, https://doi.org/10.1016/j.aca.2022.339904.
[26] Q. Pagneux, A. Roussel, H. Saada, C. Cambillau, B. Amigues, V. Delauzun, I. Engelmann, E.K. Alidjinou, J. Ogiez, A.S. Rolland, E. Faure, J. Poissy, A. Duhamel, R. Boukherroub, D. Devos, S. Szunerits, SARS-CoV-2 detection using a nanobody-functionalized voltammetric device, Commun. Med. 2 (2022) 56, https://doi.org/10.1038/s43856-022-00113-8.
[27] X. Chi, X. Zhang, S. Pan, Y. Yu, T. Lin, H. Duan, X. Liu, W. Chen, X. Yang, Q. Ding, J. Wang, W. Yang, An ultrapotent RBD-targeted biparatopic nanobody neutralizes broad SARS-CoV-2 variants, Signal Transduct. Target. Ther. (2021), https://doi.org/10.1101/2021.12.25.474052.
[28] J.-W. Zhao, Y. Li, D. Luan, X.W. (David) Lou, Structural evolution and catalytic mechanisms of perovskite oxides in electrocatalysis, Sci. Adv. 10 (2024), https://doi.org/10.1126/sciadv.adq4696.
[29] B. Huang, X. Zhou, Z. Xue, X. Lu, Electrochemiluminescence quenching of tris(2,2′-bipyridyl)ruthenium, TrAC Trends, Anal. Chem. 51 (2013) 107–116, https://doi.org/10.1016/j.trac.2013.06.012.
[30] W. Miao, Electrogenerated Chemiluminescence and Its Biorelated Applications, Chem. Rev. 108 (2008) 2506–2553, https://doi.org/10.1021/cr068083a.
[31] R.J. Forster, P. Bertoncello, T.E. Keyes, Electrogenerated chemiluminescence, Annu. Rev. Anal. Chem. 2 (2009) 359–385, https://doi.org/10.1146/annurev-anchem-060908-155305.
[32] A. Grimaud, W.T. Hong, Y. Shao-Horn, J.-M. Tarascon, Anionic redox processes for electrochemical devices, Nat. Mater. 15 (2016) 121–126, https://doi.org/10.1038/nmat4551.
[33] L. Fu, T. Song, Q. Li, G. Zou, F. Zhang, Z. Li, H. Guan, Y. Guo, Recent advances and future prospects in oxidative-reduction low-triggering-potential electrochemiluminescence strategies based on nanoparticle luminophores, Analyst 150 (2025) 34–45, https://doi.org/10.1039/D4AN01314J.
[34] K. Ino, T. Mockaitis, R. Shikuwa, K. Oba, K. Hiramoto, I. Morkvenaite-Vilkonciene, H. Abe, H. Shiku, Recent advances in electrochemiluminescence sensing for in vitro cell analysis: a review, Anal. Sci. 41 (2025) 557–569, https://doi.org/10.1007/s44211-025-00723-x.
[35] G. Moreno-Grijalva, J.C. Calva-Yáñez, A. Tirado-Guízar, V. Sarmiento, M. T. Oropeza-Guzmán, Evaluation of antigen-antibody recognition by electrochemical impedance on AuNP-biopolymer electrode, J. Appl. Electrochem. 55 (2025) 1545–1555, https://doi.org/10.1007/s10800-024-02257-y.
[36] C. Zhao, L. Niu, X. Wang, W. Sun, Electrochemiluminescence of gold nanoparticles and gold nanoparticle-labelled antibodies as co-reactants, RSC Adv. 8 (2018) 36219–36222, https://doi.org/10.1039/C8RA07429A.
[37] E. Martínez-Periñán, C. Gutiérrez-Sánchez, T. García-Mendiola, E. Lorenzo, Electrochemiluminescence biosensors using screen-printed electrodes, Biosensors 10 (2020) 118, https://doi.org/10.3390/bios10090118.
[38] S.E.K. Kirschbaum, A.J. Baeumner, A review of electrochemiluminescence (ECL) in and for microfluidic analytical devices, Anal. Bioanal. Chem. 407 (2015) 3911–3926, https://doi.org/10.1007/s00216-015-8557-x.
[39] R. Funari, K.Y. Chu, A.Q. Shen, Detection of antibodies against SARS-CoV-2 spike protein by gold nanospikes in an opto-microfluidic chip, Biosens. Bioelectron. 169 (2020) 112578, https://doi.org/10.1016/j.bios.2020.112578.
[40] J.H. Lee, M. Choi, Y. Jung, S.K. Lee, C.S. Lee, J. Kim, J. Kim, N.H. Kim, B.T. Kim, H. G. Kim, A novel rapid detection for SARS-CoV-2 spike 1 antigens using human angiotensin converting enzyme 2 (ACE2), Biosens. Bioelectron. 171 (2021) 112715, https://doi.org/10.1016/j.bios.2020.112715.
[41] W. Yin, J. Zhang, H. Wang, Y. Wang, X. Zeng, Z. Xu, J. Yang, Z. Xiao, B. D. Hammock, P. Wen, A highly sensitive electrochemical immunosensor based on electrospun nanocomposite for the detection of parathion, Food Chem. 404 (2023) 134371, https://doi.org/10.1016/j.foodchem.2022.134371.
[42] M.I.A. Ahmad, C.G. Amorim, L.F. Abu Qatouseh, M.C.B.S.M. Montenegro, Nanobody-based immunosensor for the detection of H. pylori in saliva, Biosens. Bioelectron. 260 (2024) 116423, https://doi.org/10.1016/j.bios.2024.116423.
[43] J. Hu, P. Wen, Y. Wang, J. Yang, Z. Xiao, Z. Xu, Y. Shen, H. Wang, B.D. Hammock, Fabrication of a label-free electrochemical immunosensor by functionalized nanofiber membrane for the ultrasensitive detection of quinalphos, Food Control 162 (2024) 110423, https://doi.org/10.1016/j.foodcont.2024.110423.
[44] P. Wen, Y.-Y. Yang, W.-J. Yin, J.-C. Hu, Y.-D. Shen, Y. Wang, Z.-L. Xu, Z.-L. Xiao, H.-T. Lei, J.-Y. Yang, H. Wang, B.D. Hammock, Preparation of an ultrasensitive electrochemical immunosensor for the rapid detection of 19-nortestosterone based on polyvinyl alcohol/polyacrylic acid electrospun nanofiber mat, Sens Actuators B Chem 370 (2022) 132450, https://doi.org/10.1016/j.snb.2022.132450.
[45] L. Li, X. Liu, B. Su, H. Zhang, R. Li, Z. Liu, Q. Chen, T. Huang, H. Cao, An innovative electrochemical immunosensor based on nanobody heptamer and AuNPs@ZIF-8 nanocomposites as support for the detection of alpha fetoprotein in serum, Microchem. J. 179 (2022) 107463, https://doi.org/10.1016/j.microc.2022.107463.
[46] X. Liu, D. Wang, J. Chu, Y. Xu, W. Wang, Sandwich pair nanobodies, a potential tool for electrochemical immunosensing serum prostate-specific antigen with preferable specificity, J. Pharm. Biomed. Anal. 158 (2018) 361–369, https://doi.org/10.1016/j.jpba.2018.06.021.
[47] D. Pan, G. Li, H. Hu, H. Xue, M. Zhang, M. Zhu, X. Gong, Y. Zhang, Y. Wan, Y. Shen, Direct immunoassay for facile and sensitive detection of small molecule aflatoxin B_1 based on nanobody, Chem. – A Eur. J. 24 (2018) 9869–9876, https://doi.org/10.1002/chem.201801202.
[48] T. Guerrero-Esteban, C. Gutiérrez-Sánchez, A.M. Villa-Manso, M. Revenga-Parra, F. Pariente, E. Lorenzo, Sensitive SARS-CoV-2 detection in wastewaters using a carbon nanodot-amplified electrochemiluminescence immunosensor, Talanta 247 (2022) 123543, https://doi.org/10.1016/j.talanta.2022.123543.
[49] M. Hosseini, E. Sobhanie, F. Salehnia, G. Xu, H. Rabbani, M. Naghavi Sheikholeslami, A. Firoozbakhtian, N. Sadeghi, M. Hossein Farajollah, M. Reza Ganjali, H. Vosough, Development of sandwich electrochemiluminescence immunosensor for COVID-19 diagnosis by SARS-CoV-2 spike protein detection based on Au@BSA-luminol nanocomposites, Bioelectrochem 147 (2022) 108161, https://doi.org/10.1016/j.bioelechem.2022.108161.
[50] B. Wang, X. Liu, D. Fan, H. Ma, Z. Gao, D. Wu, Q. Wei, Ultrasensitive detection of SARS-CoV-2 Nucleocapsid Protein based on porphyrin-based metal–organic gels with highly efficient electrochemiluminescence at low potential, Anal. Chem. 96 (2024) 4479–4486, https://doi.org/10.1021/acs.analchem.3c04972.
[51] J. Gong, T. Zhang, T. Luo, X. Luo, F. Yan, W. Tang, J. Liu, Bipolar silica nanochannel array confined electrochemiluminescence for ultrasensitive detection of SARS-CoV-2 antibody, Biosens. Bioelectron. 215 (2022) 114563, https://doi.org/10.1016/J.BIOS.2022.114563.
[52] S. Feng, F. Pei, W. Hu, Z. Liu, B. Du, X. Mu, B. Liu, Q. Hao, W. Lei, Z. Tong, An ultrasensitive electrochemiluminescence immunosensor for SARS-CoV-2 nucleocapsid protein detection based on signal amplification strategy of DMSN@QDs, New J. Chem. 47 (2023) 10706–10714, https://doi.org/10.1039/D3NJ01641B.
[53] H. Mohtasham, D. Bahari, A.H. Keihan, A. Salimi, R.T. Mehrebani, M. Rahimi-Nasrabadi, Magnetic N-doped carbon derived from mixed ligands MOF as effective electrochemiluminescence coreactor for performance enhancement of SARS-CoV-2 immunosensor, Talanta 277 (2024) 126252, https://doi.org/10.1016/J.TALANTA.2024.126252.
[54] E.B. Aydın, M. Aydın, M.K. Sezgintürk, New impedimetric sandwich immunosensor for ultrasensitive and highly specific detection of Spike Receptor Binding Domain Protein of SARS-CoV-2, ACS Biomater. Sci. Eng. 7 (2021) 3874–3885, https://doi.org/10.1021/acsbiomaterials.1c00580.
[55] E.B. Aydın, M. Aydın, M.K. Sezgintürk, Highly selective and sensitive sandwich immunosensor platform modified with MUA-capped GNPs for detection of spike receptor binding domain protein: a precious marker of COVID 19 infection, Sens. Actuat. B: Chem. 345 (2021) 130355, https://doi.org/10.1016/J.SNB.2021.130355.
[56] A. Erdem, H. Senturk, E. Yildiz, M. Maral, Amperometric immunosensor developed for sensitive detection of SARS-CoV-2 spike S1 protein in combined with portable device, Talanta 244 (2022) 123422, https://doi.org/10.1016/J.TALANTA.2022.123422.
[57] M. Mehmandoust, Z.P. Gumus, M. Soylak, N. Erk, Electrochemical immunosensor for rapid and highly sensitive detection of SARS-CoV-2 antigen in the nasal sample, Talanta 240 (2022) 123211, https://doi.org/10.1016/J.TALANTA.2022.123211.
[58] D. Soto, J. Orozco, Peptide-based simple detection of SARS-CoV-2 with electrochemical readout, Anal. Chim. Acta 1205 (2022) 339739, https://doi.org/10.1016/J.ACA.2022.339739.
[59] Z. Rahmati, M. Roushani, H. Hosseini, H. Choobin, An electrochemical immunosensor using SARS-CoV-2 spike protein-nickel hydroxide nanoparticles bio-conjugate modified SPCE for ultrasensitive detection of SARS-CoV-2 antibodies, Microchem. J. 170 (2021) 106718, https://doi.org/10.1016/J.MICROC.2021.106718.